Science Bulletin 63 (2018) 795–801

Contents lists available at ScienceDirect

Science Bulletin

journal homepage: www.elsevier.com/locate/scib

Article

Self-powered electrochromic devices with tunable infrared intensity

Jiangman Sun [a,1], Xiong Pu [a,b,1], Chunyan Jiang [a,b,1], Chunhua Du [a], Mengmeng Liu [a], Yang Zhang [a], Zhitian Liu [d], Junyi Zhai [a,b,*], Weiguo Hu [a,b,*], Zhong Lin Wang [a,c]

[a] CAS Center for Excellence in Nanoscience, Beijing Key Laboratory of Micro-nano Energy and Sensor, Beijing Institute of Nanoenergy and Nanosystems, Chinese Academy of Sciences, Beijing 100083, China
[b] School of Nanoscience and Technology, University of Chinese Academy of Sciences, Beijing 100049, China
[c] School of Materials Science and Engineering, Georgia Institute of Technology Atlanta, GA 30332-0245, USA
[d] Wuhan Institute of Technology Materials Science and Engineering, Wuhang 430205, China

ARTICLE INFO

Article history:
Received 14 March 2018
Received in revised form 4 April 2018
Accepted 2 May 2018
Available online 25 May 2018

Keywords:
Infrared electrochromical device
Triboelectric nanogenerator
Self-powered
Flexible
Thermal control

ABSTRACT

Triboelectric nanogenerator (TENG) is an efficient way to convert ambient mechanical energy into electricity to power up portable electronics. In this work, a flexible infrared electrochromical device (IR-ECD) with stable performances was assembled with a TENG for building self-powered infrared detector with tunable intensity. As driven by TENG, the electrochromic device could be operated in the mid-IR region due to the reversible electrochromic reactions. An average infrared reflectance contrast of 46% was achieved in 8–14 μm regions and as well a clear thermal image change can be observed. This work indicates that the TENG-driven infrared electrochromical device has potential for use in self-powered camouflage and thermal control.

1. Introduction

Inspired from animals those can change their skin colors to match the surrounding environments for camouflage, communication and temperature control, such as octopus, chameleons [1] and butterfly [2,3], materials and surfaces that imitate natural coloration mechanisms have been developed and they were promising for some commercial and military applications [4]. Similar to color changes in visible light region, the changes of infrared spectroscopy have also attracted intense attentions such as infrared camouflage, energy efficient buildings and aircraft thermal control [5,6]. Some electrochromic materials not only can provide a reversible color change of visible/near-infrared spectral regions by applying external voltage, but also show some intrinsic variation of mid- to far-IR signature. Polyaniline (PANI), as one of the most attractive conducting polymer, is widely used to construct infrared electrochromic devices (IR-ECD) with high IR contrast [7,8]. Because of the unique advantages of light weight, easy processing, flexibility and fast switching [9–13], the IR-ECDs based on PANI have promising applications in infrared camouflage or thermal control. Considering some special working environments of IR-ECD, such as outdoor operation, therefore a continuous supply of energy to drive the IR-ECD is very important.

Harvesting energy [14], such as thermal [15,16], mechanical [17–19], solar [12–24], etc., from the working environments of IR-ECDs to achieve a sustainable energy supply is obviously necessary due to some field operation. Recently, the triboelectric nanogenerator (TENG) [25–30], based on the coupling effect of contact electrification and electrostatic induction [25,26], is invented to convert mechanical energy into electricity, which has been widely used to construct the self-powered system by integrating with various devices, such as wireless sensor networks [31,32], electrochemical reactions [33,34], chemical sensors [35], home appliances [36,37] and security detection [38]. Through the strategy of rational structure design and material optimization, a variety of TENGs with higher output performance and novel characters, such as transparent and flexibility, have been developed and achieved the requirement of some special working environments [27,39–42].

In this paper, we established an IR-ECD based on PANI with a sulfuric acid dopant, which is powered by TENG [7,40]. The infrared electrochromical device used the flexible poly(ethylene terephthalate) (PET) as substrate and PANI as the electrochromic material and ion storage layer. Unlike the battery-like design where electrochromic materials are sandwiched between two electrodes,

* Corresponding authors.
E-mail addresses: jyzhai@binn.cas.cn (J. Zhai), huweiguo@binn.cas.cn (W. Hu).
[1] Jiangman Sun, Xiong Pu, Chunyan Jiang contributed equally to this work.

https://doi.org/10.1016/j.scib.2018.05.019
2095-9273/

electrochromic PANI was deposited here on the topside of a microporous polyethersulfone (PES) film with a metallic layer. The electrochemical stability and mechanical durability of the IR-ECD device were demonstrated herein, even at bending and twisting conditions. We also measured the reflectance of the IR-ECD under a variation of the potentials and took thermal images using an infrared camera. The electrochromical device exhibited an obvious reflectance contrast of 46% as PANI switched from an infrared-light transparent to an absorbing state upon reversible electrochemical doping by applying external voltage produced by a rotating TENG.

2. Experimental

2.1. Materials

Microporous PES films with a pore size of about 0.45 μm purchased from JIN TENG were used as the working electrode polymer substrate. PET films with a thickness of 110 μm purchased from DuPont Co. were used as the counter electrode flexible polymer substrate. Aniline and polyvinyl alcohol (PVA) were purchased from TCI and Aldrich, respectively.

2.2. Preparation of working and counter electrode

As shown in Fig. 1a, Au layers with a thickness of about 200 nm were deposited on the PES and PET films respectively by the DC magnetron sputtering. Then the PANI films were deposited on the Au/PES and Au/PET electrode by electrochemical polymerization. Galvanostatic condition was applied to perform all electrochemical polymerizations by the CHI 660E electrochemical workstation in this work. A three-electrode system, consisting of a reference electrode (Ag/AgCl (KCl sat.)), a working electrode, and an Au counter electrode, was used in this work. PANI was polymerized from a 1 mol/L sulfuric acid solution with an aniline concentration of 0.5 mol/L under galvanostatic condition. A 0.3 and 0.06 mA/cm^2 current densities for the Au/PES working electrode and Au/PET counter electrode were applied, respectively. Following electrochemical polymerization, the two electrode substrates were washed by deionized water and dried at 40 °C under vacuum condition.

2.3. Fabrication of the infrared electrochromic device

The electrolyte was prepared by mixing 12 wt% PVA, 6 wt% sulfuric acid and 82 wt% deionized water, followed by heating to 80 °C with stirring until PVA totally dissolved. The electrolyte was sandwiched between the working and counter electrode substrate.

2.4. Fabrication of the TENG

The TENG composed of a bottom stator and a top rotor. On the rotor board, there is a radial array of copper gratings with a length of 7.2 cm and central angle of 1°. On top of the stator, a radially interdigital structure of the two copper electrodes is covered by a Kapton thin film. Each "finger" of the underneath copper grating also has a central angle of about 1°. Once the rotor was brought into contact with the Kapton film and starts rotating, the Kapton film will be electrified and electrons will flow alternately through an external circuit between the underneath two electrodes due to the electrostatic induction effect, generating an AC output [43].

2.5. Characterization

The surface morphologies of PES film, Au/PES film and PANI/Au/PES film were examined by scanning electron microscopy (SEM, Hitachi SU8200). Electrochemical characterization of IR-ECD and the PANI film were measured by electrochemical workstation (CHI 660E). The IR absorption of PANI film and the IR reflectance of IR-ECD were measured by Fourier transform microscopic IR spectroscopy (FT-IR, VERTEX80v from Bruker). Thermal images of the device were captured using a Fortric 220, which has a spectral range of 8–14 μm. The output short current and open circuit voltage of TENG were measured by a Stanford low noise current preamplifier (Model SR570) and a Keithley electrometer (Keithley 6514), respectively.

3. Results and discussion

The construction process of IR-ECD was shown in Fig. 1a. The PANI films, deposited on Au/PES and Au/PET substrates by electrochemical polymerization, were served as the electrochromic and ion storage materials, respectively. The pore size and morphologies of pure PES film and PES film with 200-nm-thick Au layer were shown in Fig. 1. As shown in the SEM images, the pore size of pure PES film (Fig. 1b) was about 1–2 μm, and was decreased obviously after sputtering Au film (Fig. 1c). The gold was present inside the pores and therefore a good chemical resistance in the solvent of electropolymerization was achieved. As a result, a uniform PANI film covering the pores was obtained, as shown in Fig. 1d. The FT-IR spectrum of PANI film on PES/Au substrate, shown in Fig. 1e, confirmed the structure of the conducted polymer. The main IR absorption bands were assigned in Table 1. The PANI polymers have a general formula of $[(-B-NH-B-NH-)_x(-B-N=Q=N-)_{1-x}]_n$, in which B and Q denote the C_6H_4 rings in the benzenoid and quinoid forms, respectively [43]. The peaks at 1,600 and 1,560 cm^{-1} were assigned to the quinoid and benzenoid stretching deformation, respectively. Peaks around 1,455 cm^{-1} were assigned to the stretching mode of benzene ring and peak at 1,206 cm^{-1} was corresponding to C–H in-plane bending. Peaks at 1,286 and 1,131 cm^{-1} were assigned to the C–N stretching and a mode of QN^+H–B or B–NH–B, respectively. The IR spectrum suggested that the PANI film was successfully prepared on the Au/PES substrate by electrochemical polymerization.

After the construction of the stacking structured IR-ECD, which was explained in the experimental section in detail, the characterizations of IR-ECD were carried out by electrochemical workstation to evaluate the performance of the device. The redox reaction of PANI was schematically explained in Fig. 2a. During the oxidation process, ions are doped to the polymer. While a reversible reaction will occur and the ions are dedoped during the reduction reaction. The cyclic voltammetry analysis of the IR-ECD at a scanning rate of 100 mV/s for 20 cycles was shown in Fig. 2b. Reduction peak and oxidation peak appeared at −0.25 and 0.3 V respectively, which corresponded to the states transformation of PANI from the fully reduced leucoemeraldine to the 50% intrinsically oxidized polymer termed emeraldine [44]. At the additional potential of 0.8 V, the PANI working electrode was at the doping state which was defined as "green protonated emeraldine" [44], and the oxidation state was dominating. While at the potential of −0.8 V, a "colorless leucoemeraldine" [45] was observed as the process of dedoping. In addition, the switching time of the IR-ECD was also measured as applying constant potential of 0.8 or −0.8 V. From Fig. 2c, it can be observed that the response time, which was defined as the total time of the abrupt change of current, was as fast as 5 s. When a potential of 0.8 V was added, the current decreased from 35 to 0.4 mA and then kept at 0.4 mA. A similar result can be observed when a potential of −0.8 V was added. Then we studied the performance of the device driven by the electrochemical workstation under 2 mA constant current (Fig. 2d), a time about 25 s was spent when the voltage changed from −0.8 to 0.8 V.

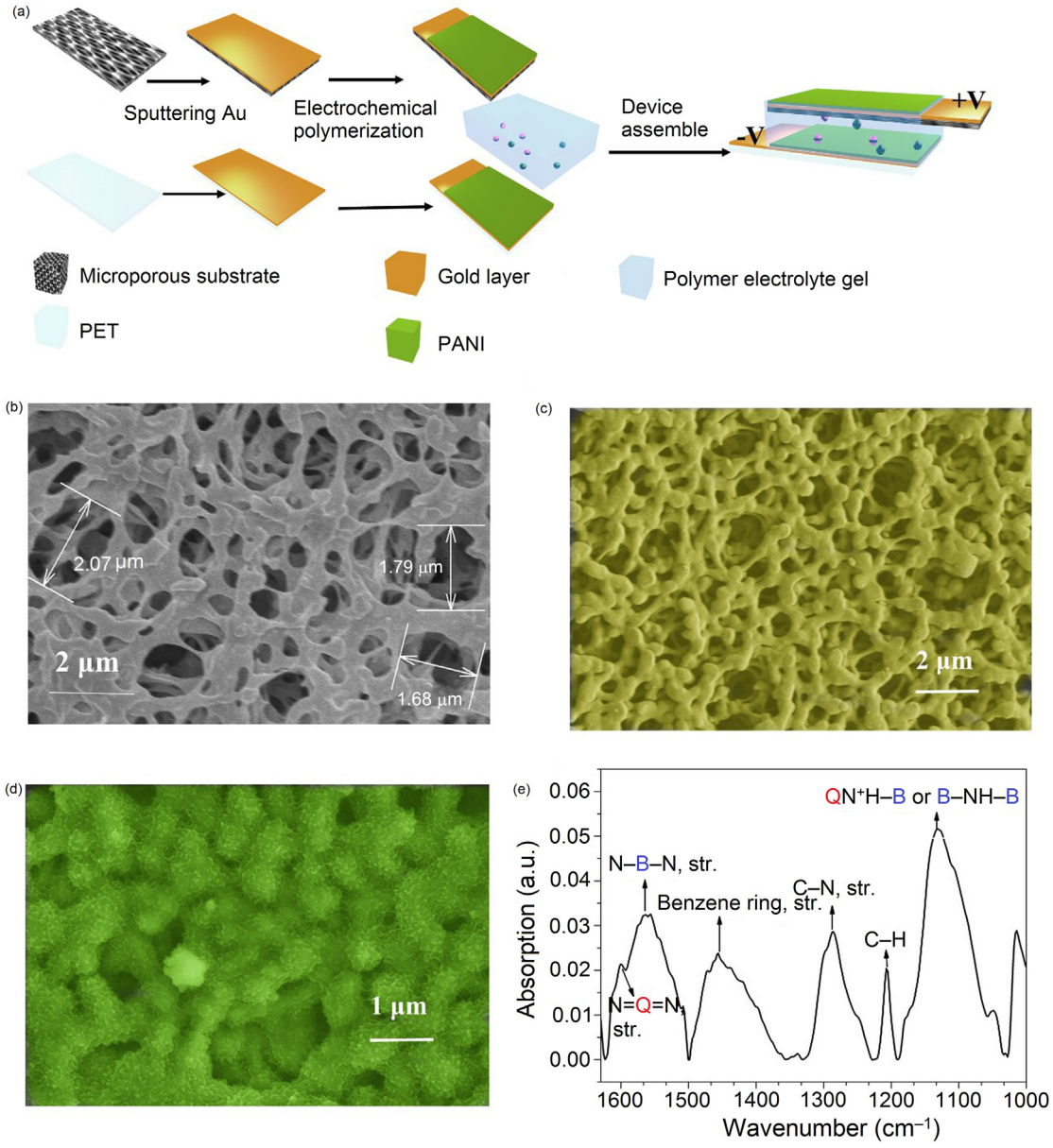

Fig. 1. (Color online) (a) Schematic representation of the infrared electrochromic device. SEM images of microporous PES film (b), 200 nm thicker Au layer on PES film (c) and electrochemical polymerized PAIN film on the composite Au/PES substrate (d). (e) IR spectrum of the electrochemical polymerized PANI film on PES/Au substrate.

Table 1
Assignments for IR absorption bands for electrochemical polymerized PANI film.

Frequency (cm^{-1})	Assignment
1,600	Str. of N=Q=N
1,560	Str. of N–B–N
1,455	Str. of benzene ring
1,286	Str. of C–N
1,206	C–H in-plane bending
1,131	A mode of $QN^{+}H$–B or B–NH–B

Str., stretching.
B, benzenoid unit.
Q, quinonoid unit.

The IR-ECD can be termed as an electrochemical capacitor. When a constant current of 2.0 mA was applied to the IR-ECD repeatedly with alternative reverse polarizations, the equivalent capacitance retention of 99% for 100 cycles (Fig. 2e). This electrochemical stability indicates that the redox reactions of PANI are highly reversible and nearly no degradation of the device is observed in the cycling test. From the inset of Fig. 2e, it can be seen that the voltage profiles after 100 cycles kept the same shape with that of the initial cycle, and showed no significant degradation. Therefore, it indicated that the IR-ECD can be utilized at different IR states repeatedly.

As a flexible device, the durability of the IR-ECD has been examined under strain conditions such as bending or twisting. The flexible IR-ECD device can be bended, twisted, and attached to the skin of human finger, which demonstrates the excellent flexibility of the IR-ECD device (Fig. 3a). Moreover, a series of flexibility tests were carried out under different forms of deformations. As shown in Fig. 3b, no obvious degradation of galvanostatic voltage profiles at 2 mA can be observed when the planar IR-ECD device was bent or twisted at different angles (90° and 180°), which indicated the mechanical stability of the flexible IR-ECD device. Then the device was bent to 90° for 1,000 cycles by a linear motor. And a capacitance retention of 95%, compared with the initial capacitance,

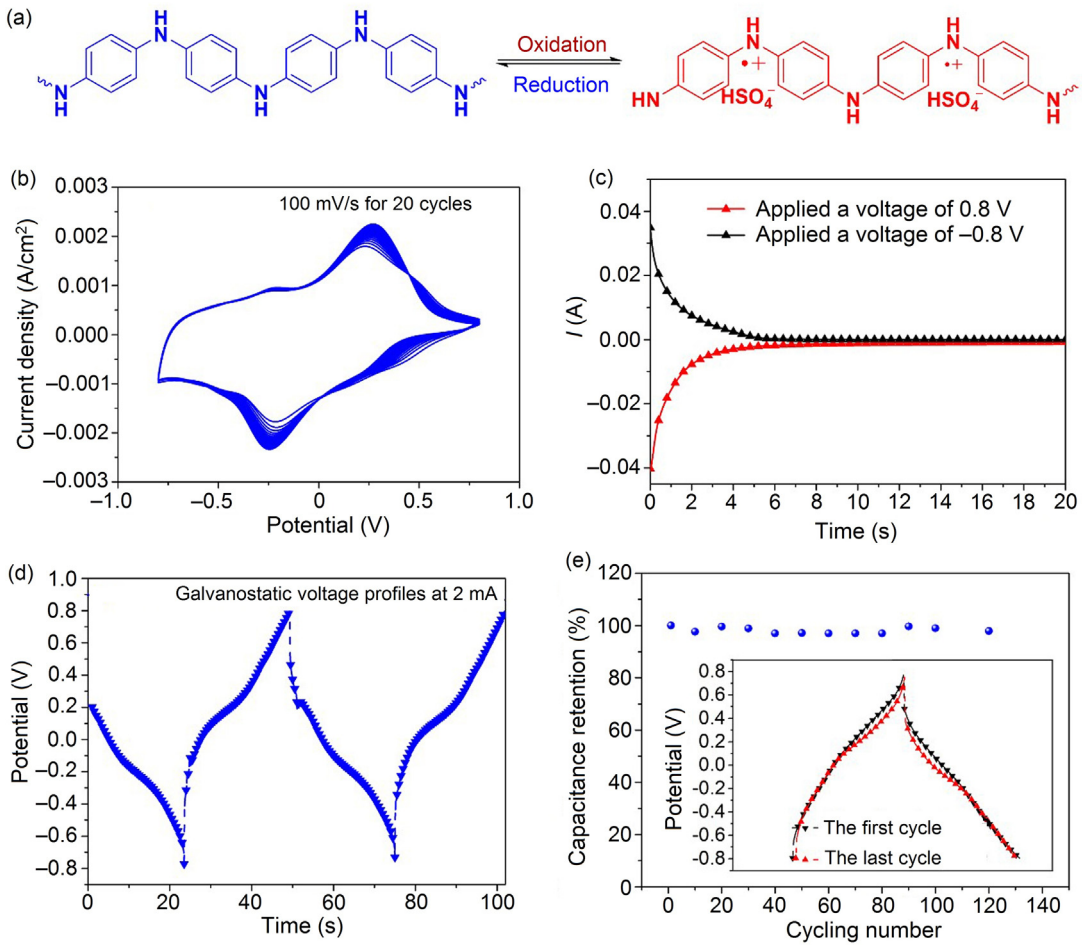

Fig. 2. (Color online) (a) Potential-induced charge redistribution of PANI at dedoped and doped states. (b) Cyclic voltammogram of 20 cycles of the IR-ECD. (c) Time dependence of current for IR-ECD under different potentials. (d) Time dependence of potential for the IR-ECD under 2 mA constant current. (e) Cycling performance of the IR-ECD at a constant current of 2 mA. The inset shows voltage profiles of the first cycle and the last cycle.

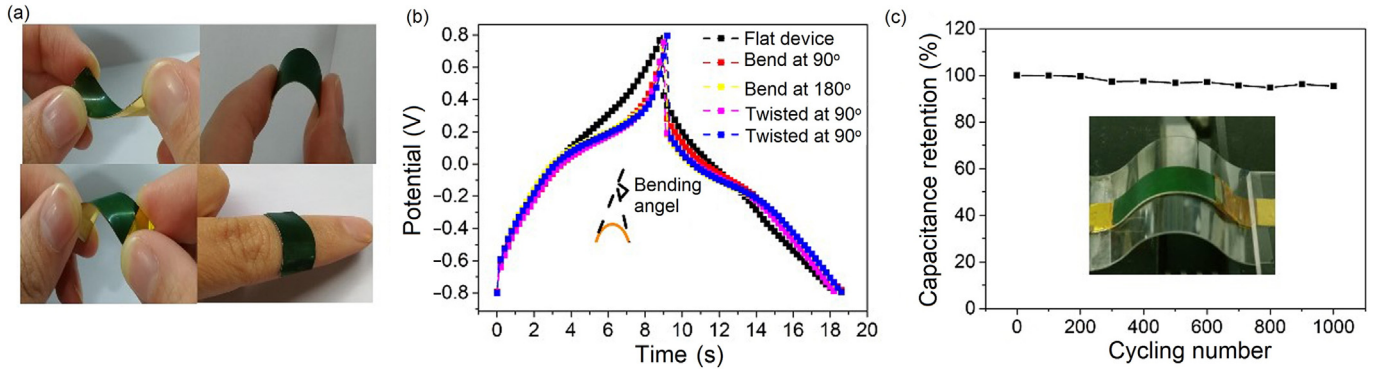

Fig. 3. (Color online) (a) Optical images of a IR-ECD bent/twisted with hands, and conformally attached on the skin of a finger. (b) Galvanostatic voltage profiles obtained under different bending and twisting angles at 2 mA constant current. (c) Capacitance retention as a function of bent cycles at a constant current of 2 mA. The inset shows the device bent by a linear motor.

was maintained after 1,000 bending cycles by the galvanostatic test, as shown in Fig. 3c. The inset in Fig. 3c shows a photo of the bent flexible IR-ECD device fixed on the linear motor. These tests confirmed the durability of the flexible IR-ECD device, which is mainly due to the use of the flexible substrate, robust adhesion of polymer active layer and the gel electrolyte.

To study the infrared electrochromic characteristics of the device, an in situ microscopic IR reflectance of the device at different potentials was carried out and shown in Fig. 4a. Due to the different electrochemical doping states of PANI at different potentials, the IR reflectance of the device varied as the potential changes. At −0.8 V, PANI was at its reduced state, the device displayed near infrared transparent (Fig. 4c). While at 0 and 0.8 V, PANI was at slightly doped and doped state, respectively, the device displayed dark green (Fig. 4d) and the IR reflectance of the device became lower. The long-wavelength infrared spectrum of 8–14 μm is one of the infrared atmospheric windows. The infrared radiation spectrums emitted by objects are absorbed little by atmosphere in the

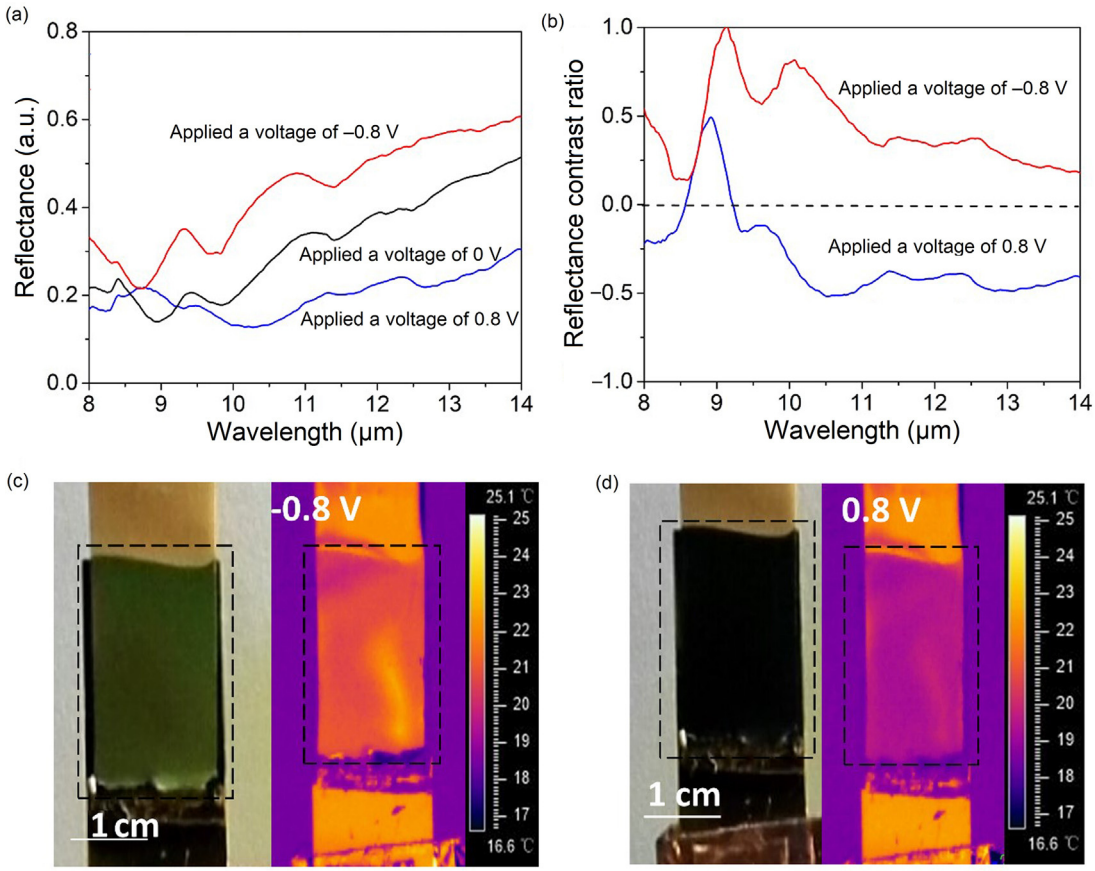

Fig. 4. (Color online) IR reflectance spectrum (a) and contrast ratio (b). Thermal images of the IR-ECD under potential of −0.8 V (c) and 0.8 V (d).

infrared atmospheric window. Therefore, the wavebands of infrared systems are always in the atmospheric windows and the spectrum of 8–14 μm is the mainly working waveband of thermal imaging system. While the IR-ECD device has a high IR reflectance contrast in the spectral regions of 8–14 μm. The average reflectance contrast calculated from Fig. 4a is about 46% in 8–14 μm regions between 0.8 and −0.8 V. Then we also calculated the reflectance contrast ratio $[(R-R_0)/R_0]$ from the infrared reflectance of 0.8 and −0.8 V respectively, where R indicated the reflectance at different applied potentials and R_0 indicated the reflectance at initial potential (0 V) (Fig. 4b). As shown in Fig. 4b, an obvious reflectance contrast ratio existed between −0.8 and 0.8 V. The highest reflectance contrast ratio of −0.8 and 0 V was about 100% at the wavelength about 9 μm and the lowest one of 0.8 and 0 V was about −50% at the wavelength about 10.5 μm. For further study on the characteristic of the IR-ECD, we also measured the thermal images of the device which were shown in Fig. 4d. The temperature of the doped state at 0.8 V and the reduced state at −0.8 V of the IR-ECD, which were measured in less than 1 min after the adding of potentials, were obviously different. Just agreeing with the microscopic IR reflectance spectra results (Fig. 4a), thermal images also revealed that the reduced state (−0.8 V) of PANI film is much more infrared transparent than its doped state. When a potential of 0.8 V was added, the color of the IR-ECD device was similar to the background (Fig. 4d).

Subsequently, the TENG described above was integrated with the IR-ECD and the optical image and schematic diagram were shown in Fig. 5a. The output of TENG was initially transformed and rectified. The output of the TENG at 250 r/min was shown in Fig. 5b and c. The open circuit voltage (V_{OC}) had a shape to the triangular wave with amplitude averaged at about 151 V, as shown in Fig. 5b. The short circuit current (I_{SC}) was a sinusoidal wave with amplitude of about 1.5 mA (Fig. 5c). The alternative output of the TENG can be converted into direct current with a rectifier. As shown in Fig. 5c, the equivalent DC current for generating the same quantity of charges can be calculated by $I_{eq} = 2I_{peak}/\pi$, which is independent of the frequency of the AC current and rectified current of the TENG, the I_{eq} of which is about 0.96 mA.

A IR-ECD with the shape of four letters "BINN" was used. The letter-shaped IR-ECD was fabricated by applying a mask on top of the microporous PES substrate when sputtering Au. Arbitrary patterns of electrochromical PANI electrode can be then facilely realized. As shown in Fig. 5d, when the TENG was connected to the IR-ECD to supply a negative current, and the electrochromic PANI letters converted from doped to reduced state in about 50 s; when the TENG was connected reversely to the IR-ECD, 50 s was spent for the IR-ECD back to doped state. Repetitive electrochromic transformations can also be powered by the TENG. The visible-light and infrared thermal images were also shown in Fig. 5e and f, indicating the color switching and temperature variations of the IR-ECD driven by TENG. These results provide reliable evidence that the IR-ECD could be powered by TENG successfully and it is hopeful to construct a self-powered infrared electrochromic system for the application of camouflage or machine thermal control.

4. Conclusion

In summary, we demonstrated the concept of a self-powered infrared electrochromic system by assembling a flexible IR-ECD with a TENG successfully. The TENG can take advantage of mechanical energy generated by the machine itself, such as the

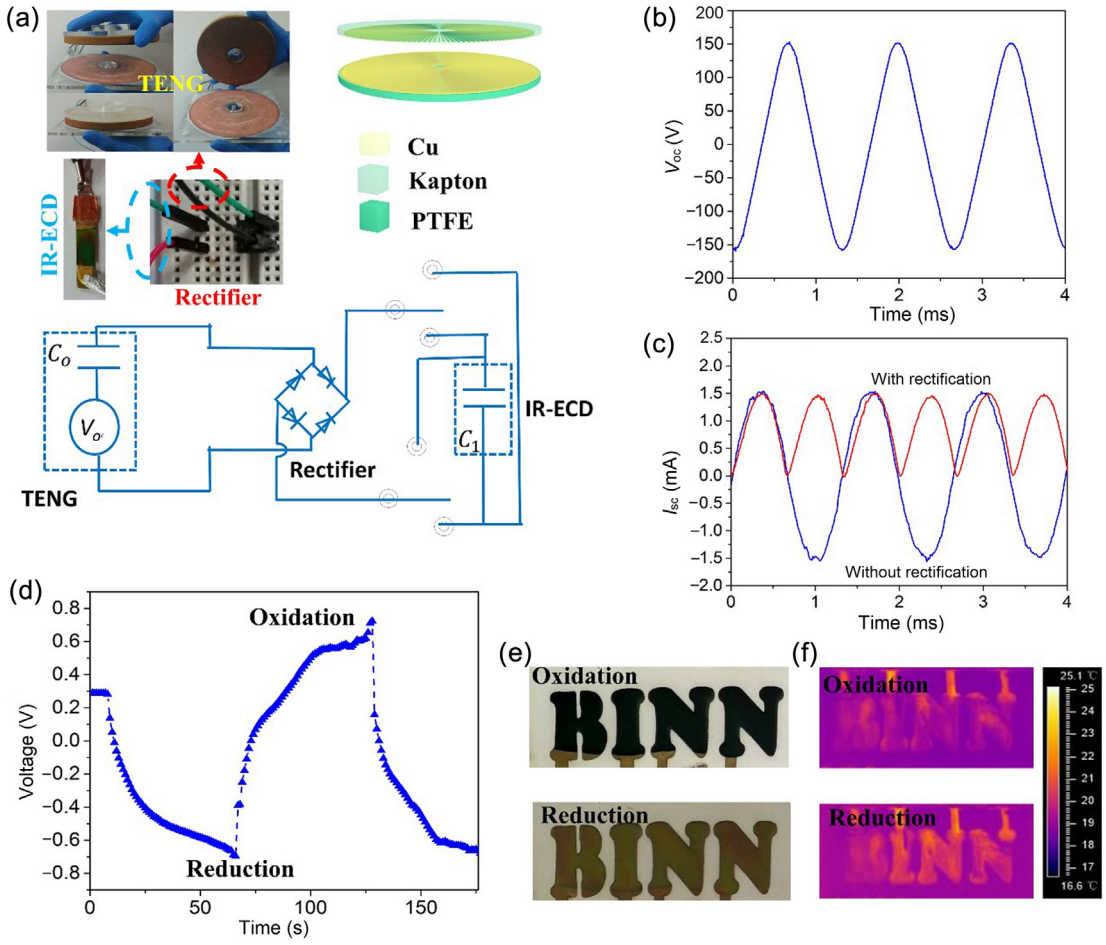

Fig. 5. (Color online) (a) The optical image and scheme of TENG driving IR-ECD. Output V_{OC} (b) and output I_{SC} (c) of the TENG. (d) Time dependence of potential for the IR-ECD under pulsed current generated by the TENG. Visible-light images (e) and thermal images (f) of the IR-ECD under different potentials.

rotational turbine or wheel, then drive an electrochromic device which could be operated in the mid-IR range. Reversible electrochromic reactions can be driven by the TENG, and an average reflectance contrast of 46% in 8–14 μm regions as well as a thermal image difference can be observed. Therefore, the TENG-driven infrared electrochromic is a meaningful attempt for self-powered IR electrochromic system which has great potential for use in camouflage and thermal control.

Conflict of interest

The authors declare that they have no conflict of interest.

Acknowledgments

This work was supported by the "Thousands Talents" Program for Pioneer Researcher and his Innovation Team, the National Key Research and Development Program from Ministry of Science and Technology of China (2016YFA0202703) , the National Natural Science Foundation of China (51432005), Hubei Technology Innovation Major Project (2016AAA030), and Petro China Innovation Foundation (2015D-5006-0211). The revised work and supplementary experiment were mainly done by Chunyan Jiang.

Appendix A. Supplementary data

Supplementary data associated with this article can be found, in the online version, at https://doi.org/10.1016/j.scib.2018.05.019.

References

[1] Yu CJ, Li YH, Zhang X, et al. Adaptive optoelectronic camouflage systems with designs inspired by cephalopod skins. Proc Natl Acad Sci USA 2014;111:12998–3003.
[2] Huang JY, Wang XD, Wang ZL, et al. Controlled replication of butterfly wings for achieving tunable photonic properties. Nano Lett 2006:62325–31.
[3] Fang Y, Sun G, Bi YH, et al. Multiple-dimensional micro/nano structural models for hydrophobicity of butterfly wing surfaces and coupling mechanism. Sci Bull 2015;60:256–63.
[4] Xiao L, Ma H, Liu J, et al. Fast adaptive thermal camouflage based on flexible VO_2/graphene/CNT thin films. Nano Lett 2015;15:8365–70.
[5] Han T, Bai X, Thong JT, et al. Full control and manipulation of heat signatures: cloaking, camouflage and thermal metamaterials. Adv Mater 2014;26:1731–4.
[6] Phan L, Walkup WG, Ordinario DD, et al. Reconfigurable infrared camouflage coatings from a cephalopod protein. Adv Mater 2013;25:5621–5.
[7] Li H, Xie K, Pan Y, et al. Variable emissivity infrared electrochromic device based on polyaniline conducting polymer. Synth Met 2009;159:1386–8.
[8] Li H, Xie K, Pan Y, et al. Study of the mechanism of the variable emissivity infrared electrochromic device based on polyaniline conducting polymer. Synth Met 2012;162:22–5.
[9] Beaujuge PM, Reynolds JR. Color control in π-conjugated organic polymers for use in electrochromic devices. Chem Rev 2010;110:268–320.
[10] Sapp SA, Sotzing GA, Reynolds JR. High contrast ratio and fast-switching dual polymer electrochromic devices. Chem Mater 1998;10:2101–8.
[11] Argun AA, Cirpan A, Reynolds JR. The first truly all-polymer electrochromic devices. Adv Mater 2003;15:1338–41.
[12] Heuer HW, Wehrmann R, Kirchmeyer S. Electrochromic window based on conducting poly(3,4-ethylenedioxythiophene)-poly(styrene sulfonate). Adv Funct Mater 2002;12:89–94.
[13] Kim B, Koh JK, Park J, et al. Patternable PEDOT nanofilms with grid electrodes for transparent electrochromic devices targeting thermal camouflage. Nano Convergence 2015;2:19–26.
[14] Pu X, Liu M, Li L, et al. Wearable textile-based in-plane microsupercapacitors. Adv Mater 2016;28:98–105.

[15] DiSalvo JF. Thermoelectric cooling and power generation. Science 1999;285:703–6.
[16] Bell EL. Cooling, heating, generating power, and recovering waste heat with thermoelectric systems. Science 2008;321:1457–61.
[17] Wang ZL, Song J. Piezoelectric nanogenerators based on zinc oxide nanowire arrays. Science 2006;312:242–6.
[18] Wang ZL. Progress in piezotronics and piezo-phototronics. Adv Mater 2012;24:4632–46.
[19] Hu Y, Wang ZL. Recent progress in piezoelectric nanogenerators as a sustainable power source in self-powered systems and active sensors. Nano Energy 2015;14:3–14.
[20] Lee YH, Kim JS, Noh J, et al. Wearable textile battery rechargeable by solar energy. Nano Lett 2013;13:5753–61.
[21] Zhang Z, Chen X, Chen P, et al. Integrated polymer solar cell and electrochemical supercapacitor in a flexible and stable fiber format. Adv Mater 2014;26:466–70.
[22] Yang Z, Deng J, Sun H, et al. Self-powered energy fiber: energy conversion in the sheath and storage in the core. Adv Mater 2014;26:7038–42.
[23] Dong YF, Wu ZS, Ren WC, et al. Graphene: a promising 2D material for electrochemical energy storage. Sci Bull 2017;62:724–40.
[24] Xiao Z, Jia X, Ding LM. Ternary organic solar cells offer 14% power conversion efficiency. Sci Bull 2017;62:1562–4.
[25] Fan FR, Tian ZQ, Wang ZL. Flexible triboelectric generator. Nano Energy 2012;1:328–34.
[26] Wang ZL. Triboelectric nanogenerators as new energy technology for self-powered systems and as active mechanical and chemical sensors. ACS Nano 2013;7:9533–57.
[27] Pu X, Li L, Song H, et al. A Self-charging power unit by integration of a textile triboelectric nanogenerator and a flexible lithium-ion battery for wearable electronics. Adv Mater 2015;27:2472–8.
[28] Tang W, Jiang T, Fan FR, et al. Liquid-metal electrode for high-performance triboelectric nanogenerator at an instantaneous energy conversion efficiency of 70.6%. Adv Funct Mater 2015;25:3718–25.
[29] Yu A, Zhao Y, Jiang P, et al. A nanogenerator as a self-powered sensor for measuring the vibration spectrum of a drum membrane. Nanotechnology 2013;24:055501.
[30] Yu A, Jiang P, Wang ZL. Nanogenerator as self-powered vibration sensor. Nano Energy 2012;1:418–23.
[31] Wang S, Lin L, Wang ZL. Nanoscale triboelectric-effect-enabled energy conversion for sustainably powering portable electronics. Nano Lett 2012;12:6339–46.
[32] Tang W, Meng B, Zhang H. Investigation of power generation based on stacked triboelectric nanogenerator. Nano Energy 2013;2:1164–71.
[33] Zhu G, Pan C, Guo W, et al. Triboelectric-generator-driven pulse electrodeposition for micropatterning. Nano Lett 2012;12:4960–5.
[34] Yang X, Zhu G, Wang S, et al. A self-powered electrochromic device driven by a nanogenerator. Energy Environ Sci 2012;5:9462–6.
[35] Lin ZH, Zhu G, Zhou YS, et al. A self-powered triboelectric nanosensor for mercury ion detection. Angew Chem Int Ed 2013;52:5065–9.
[36] Zhu G, Chen J, Zhang T, et al. Radial-arrayed rotary electrification for high performance triboelectric generator. Nat Commun 2014;5:3426–34.
[37] Zhu G, Zhou YS, Bai P, et al. A shape-adaptive thin-film-based approach for 50% high-efficiency energy generation through micro-grating sliding electrification. Adv Mater 2014;26:3788–96.
[38] Zhu G, Yang WQ, Zhang T, et al. Self-powered, ultrasensitive, flexible tactile sensors based on contact electrification. Nano Lett 2014;14:3208–13.
[39] Pu X, Li L, Liu M, et al. Wearable self-charging power textile based on flexible yarn supercapacitors and fabric nanogenerators. Adv Mater 2016;28:98–105.
[40] Pu X, Liu M, Li LX, et al. Efficient charging of Li-ion batteries with pulsed output current of triboelectric nanogenerators. Adv Sci 2016;3:1500255.
[41] Kim S, Gupta MK, Lee KY, et al. Transparent flexible graphene triboelectric nanogenerators. Adv Mater 2014;26:3918–25.
[42] Ko YH, Nagaraju G, Lee SH, et al. PDMS-based triboelectric and transparent nanogenerators with ZnO nanorod arrays. ACS Appl Mater Interfaces 2014;6:6631–7.
[43] Han C, Zhang C, Tang W, et al. High power triboelectric nanogenerator based on printed circuit board (PCB) technology. Nano Res 2015;8:722–30.
[44] Kang ET, Neoh KG, Tan KL. Polyaniline: interesting a polymer with many intrinsic redox states. Prog Polym Sci 1998;23:211–324.
[45] Stejskal J, Kratochvil P, Jenkins AD. Polyaniline: forms and formation. Collect Czech Chem Commun 1995;60:1747–55.

Jiangman Sun received her Ph.D. from South China University of Technology and then joined Centra for High Pression Science & Technology Advanced Research (HPSTAR) as a postdoctoral fellow. Now she is a post-doctoral fellow at Beijing Institute of Nanoenergy and Nanosystems, Chinese Academy of Sciences. Her research focuses on conjugated polymers and elastomers.

Weiguo Hu is a principle investigator at Beijing Institute of Nanoenergy and Nanosystems, Chinese Academy of Sciences. His research focuses on III-nitrides piezotronic/piezophototronic devices, and flexible energy and electronic devices.

Junyi Zhai received his Ph.D. from Virginia Polytechnic Institute and State University (2009) and then joined Los Alamos National Laboratory (LANL) as a postdoctoral fellow. Now, he is full Professor and group leader at Beijing Institute of Nanoenergy and Nanosystems, Chinese Academy of Sciences. His main research interests and activities are micro/nanopiezoelectric semiconductor materials and the magnetic-mechanical-electrical-optical coupling effect.